Reactivity of Trimethyltin Manganese Pentacarbonyl in Zeolite Cavities

Aticha Borvornwattananont† and Thomas Bein*

Department of Chemistry, Purdue University, West Lafayette, Indiana 47907 *(Received: June 22, 1992)*

The anchoring chemistry, thermal stability, and reactivity of $Me_3SnMn(CO)_5$ in zeolite NaY and acid forms of zeolite Y was studied with X-ray absorption spectroscopy (Sn, Mn edge EXAFS) and in situ FTIR/TPD-MS techniques. In the NaY host, the precursor is physically adsorbed from hexane solution into the dehydrated zeolite cages at room temperature without further chemical reaction. Symmetry changes of the $Mn(CO)_5$ moiety indicate interaction with the Na^+ ions of the zeolite framework. The intrazeolite complex in NaY is accessible to external reactants and undergoes carbonyl substitution with PEt_3 at the manganese center. At 393 K under vacuum, the Mn–*C*O (N = 3.9, R = 1.79 Å) and Mn–C*O* coordination (N = 4.3, R = 2.96 Å) derived from EXAFS data shows that most of the CO coordination sphere is still intact. The intrazeolite complex decomposes at about 423 K by loss of all CO ligands and, subsequently, cleavage of the Sn–Mn bond. Mn and Sn cluster species are formed at 523 K. In contrast to NaY, the acidic HY host interacts with the Me_3Sn moiety of the bimetallic complex. The compound attaches to the zeolite framework at the oxygen rings of the supercage already at room temperature. The attachment of the molecule occurs through the Sn moiety by loss of CH_4 gas while the Sn–Mn bond and the CO ligand sphere are still intact. Different degrees of substitution of the methyl groups by the acidic oxygen framework are observed. Both mono- and disubstituted species, $(Oz)Me_2SnMn(CO)_5$ and $(Oz)_2MeSnMn(CO)_5$, are formed under retention of the Sn–Mn bond. At room temperature, the monosubstitution is favored while disubstitution is more pronounced at higher temperature, i.e., 373 K. At this temperature, the Mn–CO coordination data still indicate five CO ligands (Mn–*C*O, R = 1.84 Å, Mn–C*O*, R = 2.97 Å), and the Sn–Mn bond is still intact (N = 0.9, R = 2.58). After the Sn–Mn bond is cleaved at 423 K, Sn is still anchored to the zeolite framework through oxygen coordination while Mn cluster species are formed. At 523 K, both Sn and Mn are attached to the zeolite oxygen framework.

Introduction

The quest for well-defined, stable hybrid catalysts containing organometallic species continues.[1,2] Facile separation of the products from the catalyst as well as novel means to enhance selectivity are important promising features of hybrid catalysts. The crystalline channel systems of zeolites (open framework oxide structures with pore sizes between 0.3 and 1.2 nm and exchangeable cations)[3,4] are particularly attractive hosts for the design of hybrid systems because they are structurally much better defined than amorphous supports. For instance, the regular pore size can be a means to control diffusional access of reactants to the catalytic centers. However, complications encountered with zeolite-based and other hybrid systems can involve leaching of the catalyst into solution or instability of the metal phase against agglomeration.

In the context of our program aimed at the development of immobilization concepts for organometallic fragments in microporous solids, this article describes a comprehensive study on the attachment chemistry and reactivity of $Me_3SnMn(CO)_5$ in zeolite cages.

Different strategies for the deposition of catalytically active organometallics into zeolites include physisorption of neutral metal carbonyls,[5,6] diffusional blocking of phtalocyanine (Pc) and other chelate complexes,[7,8] and ligation at transition-metal cations such as formation of Rh carbonyl complex cations.[9,10] Migration and agglomeration of the intrazeolite Rh species appears to occur under the experimental conditions used for catalytic hydroformylation reactions.[11]

Improved stability of the intrazeolite species should be expected from surface-attached complexes that utilize the bridging zeolite hydroxyls for anchoring reactions, such as the reaction of $Rh(allyl)_3$ with partially proton-exchanged X and Y type zeolite.[12-15] The formation of intrazeolite Rh–CO and -hydride species as inferred from infrared data indicated that the anchored Rh–allyl fragment reacted similar to the complex in solution.

We explore a new approach by introducing *heterobinuclear* organometallics as candidates for linking catalytic functions to the zeolite framework. If two metal centers are present, the complex can be "anchored" to the support via one appropriately chosen, oxophilic metal, whereas the catalytic reaction may proceed at the second metal center. We could recently demonstrate the new bimetallic approach by utilizing the intrazeolite attachment chemistry of Ge–transition metal complexes.[16] Framework attachment of $Cl_2(THF)GeMo(CO)_5$ and $Cl_2(THF)GeW(CO)_5$ was possible in both the Na form of zeolite Y and in the proton-exchanged form. Both compounds react with the acidic zeolite at elevated temperatures under removal of chloride ligands.

In this article, we discuss the different surface chemistry and stability of $Me_3SnMn(CO)_5$ in similar zeolite supports. The stability of the Sn–Mn bond in this compound under different conditions has been studied in detail. Upon treatment of $Me_3SnMn(CO)_5$ with hydrogen halides, such as HCl, HBr and HI, either with or without organic solvents, formation of $X_nMe_{3-n}SnMn(CO)_5$ in high yield was observed under retention of the Sn–Mn bond.[17] The degree of methyl substitution depends on the stoichiometry of the acids versus the organometallic compound. The stability of the Sn–Mn bond toward these acids is of great interest in this context. The tin atom behaves as a π-acceptor (σ-donor) in $Me_3SnMn(CO)_5$ and in many organometallics. The considerable strength of the Sn–Mn bond compared to its group IV analogues is assumed to be due to a $d\pi$–$d\pi$ interaction between the Sn and Mn atoms.[18] If a proton-exchanged zeolite is considered to be a solid acid, similar substitution reactions as in solution are expected to occur. The methyl ligand is a good leaving group on attack with Bronsted acids to form stable methane. Thus, the zeolite framework will not be at risk to be attacked by the leaving species as in the case of HCl. This is an important advantage of $Me_3SnMn(CO)_5$ compared to the surface chemistry of the dichlorogermylene compounds mentioned above.

The precursor is expected to react with the internal surface hydroxyl groups of the zeolites by loss of methane gas, whereas the Sn–Mn bond and the coordination sphere of Mn should remain intact. The substitution of the methyl groups requires other ligands at the Sn moiety, i.e., most likely the metal–oxygen rings of the zeolite framework. The present article describes a detailed analysis of the anchoring process and the stability of the intrazeolite species as a function of zeolite acidity and temperature and their reactivity toward other ligands.

Experimental Section

Sample Preparation. All manipulations were carried out under nitrogen atmosphere. Prior to each measurement, samples were kept in a nitrogen glovebox. The precursor $Me_3SnMn(CO)_5$ (mp

†Present address: Department of Chemistry, Faculty of Science, Chulalongkorn University, Bangkok 10330, Thailand.
*Author for correspondence.

0022-3654/92/2096-9447$03.00/0 © 1992 American Chemical Society

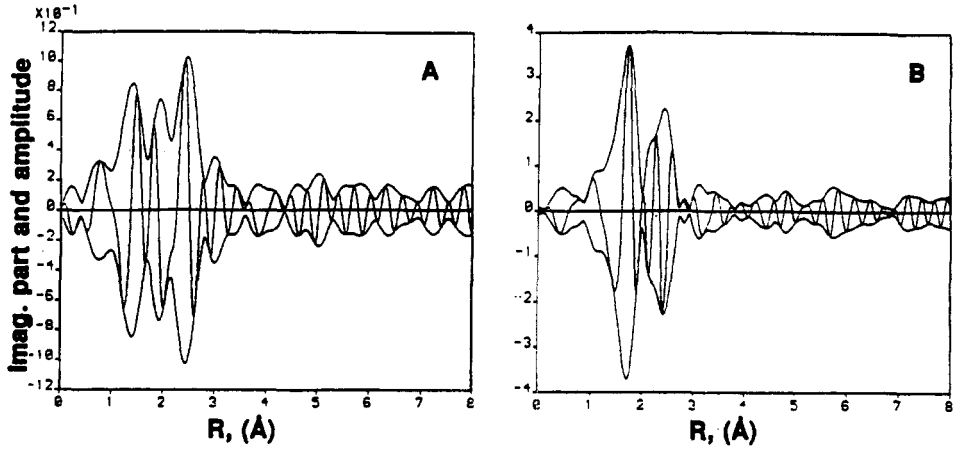

Figure 1. FT of EXAFS samples. $Me_3SnMn(CO)_5$ precursor: (A) Mn edge spectra: FT = k^2, 3.2–12 Å^{-1}, at room temperature (RT); (B) Sn edge spectra: FT = k^2, 2.6–13 Å^{-1}, at RT.

TABLE I: Crystallographic Data of Reference Compounds

material	atom pair	R (Å)	N	ref
$Mn_2(CO)_{10}$	Mn–CO	1.82	5	*a*
	Mn–*C*O	2.98	5	
	Mn–Mn	2.92	1	
Mn Foil	Mn–Mn	between 2.24 and 2.96	16	*b*
	Mn–Mn		16	
	Mn–Mn		13	
	Mn–Mn		12	
MnO_2	Mn–O	1.89	6	*c*
	Mn–Mn	2.87	2	
	Mn–O	3.48	4	
MnS	Mn–S	2.61	6	*d*
	Mn–Mn	3.68	12	
	Mn–S	6.02	8	
created $Mn(CO)_5$	Mn–CO	1.82	5	*e*
	Mn–*C*O	2.98	5	
SnO_2	Sn–O	2.07	6	*f*
Sn foil	Sn–Sn	3.02	4	*g*
	Sn–Sn	3.18	2	
$Me_3SnMn(CO)_5$	Sn–Me	2.06	1	*h*
	Sn–Me	2.16	1	
	Sn–Me	2.16	1	
	Sn–Mn	av 2.13	1	
	Mn–CO	1.81	5	
	Mn–*C*O	2.95	5	

[a] Dahl, L. F.; Rundle, R. E. *Acta Crystallogr.* **1963**, *16*, 419. [b] Bailar, J. C., Jr.; Emeleus, H. J.; Nyholm, R.; Trotman-Dickenson, A. F. *Comprehensive Inorganic Chemistry*; Pergamon Press: Oxford, 1973; Vol. 3, p 779. [c] Ewald, Von P. P.; Hermann, C. *Zeitschrift Fur Kristallographie Kristallgeometrie, Kristallphysik, Kristallchemie*, subtitle *Strukturbericht*; Johnson Reprint Corp.: New York, 1931; Vol. 1, p 155. [d] *Ibid.*, pp 73–74. [e] The same values as $Mn_2(CO)_{10}$; see supplementary material for the procedure. [f] Bailar, J. C., Jr.; Emeleus, H. J.; Nyholm, R.; Trotman-Dickenson, A. F. *Comprehensive Inorganic Chemistry*; Pergamon Press: Oxford, 1973; Vol. 2, p 53. [g] Wells, A. F. *Structural Inorganic Chemistry*, 5th ed.; Clarendon Press: Oxford, 1984; pp 1279. [h] Bryan, R. F. *J. Chem. Soc. A* **1968**, 696.

302.5 K) was synthesized from the reaction between $NaMn(CO)_5$ and Me_3SnCl in THF following a reported method[19] using the Schlenk technique.

The IR absorption in the CO region presents three bands at 2090 (m), 1996 (sh), and 1992 (vs) cm^{-1}, in hexane (reported: 2089, 1998, and 1991 cm^{-1}, in hexane[19]). Proton NMR data show one resonance at δ_{Me} = 0.46 ppm with $J_{^{119}Sn-CH}$ = 48.1 Hz and $J_{^{117}Sn-CH}$ = 46.4 Hz (reported data: δ_{Me} = 0.46 ± 0.01 ppm with $J_{^{119}Sn-CH}$ = 48.8 ± 0.2 Hz and $J_{^{117}Sn-CH}$ = 46.3 ± 0.2 Hz[19]). The mass spectrum of the compound does not show many fragments; neither the molecular mass (M), the fragmentation of M – $(CO)_m$ $Sn(CH_3)_4$, or other Sn fragments are observed. The dominant fragments CO (mass 28) and Mn (mass 55) are observed at 327 K.

The structural features of the precursor $Me_3SnMn(CO)_5$ were determined by EXAFS spectroscopy at both the Mn edge and Sn edge. The k^2-weighted Fourier transforms of $Me_3SnMn(CO)_5$ are shown in Figure 1. Crystallographic data of the reference compounds used for this and the other samples are listed in Table I. Structural information derived from the EXAFS data is presented in Table II (Mn edge) and in Table III (Sn edge). The results agree well with the expected coordination numbers and bond distances in this compound.

TABLE II: EXAFS Data Derived from the Mn Edge

sample	atom pair	N^a	R/Å^b	$\Delta\sigma^2$/Å^{2,c}	ΔE/eV^d
	$Me_3SnMn(CO)_5$ Precursor				
SnM	Mn–CO	4.8	1.85	–0.0015	–0.3
	Mn–*C*O	5.5	2.97	–0.0015	0.7
	Mn–*C*O[e]	4.7	2.95	–0.0063	1.2
	Mn–Sn	1.3	2.80	–0.0042	5.0
	$Me_3SnMn(CO)_5$ in NaY				
SnMNa/RT	Mn–CO	4.3	1.83	0.0042	0.2
	Mn–*C*O	6.0	2.97	–0.0012	0.1
SnMNa/393	Mn–CO	3.9	1.79	0.0017	0.4
	Mn–*C*O	4.3	2.96	–0.0022	0.6
SnMNa/423	Mn–O	2.7	1.95	0.0130	7.1
	Mn–Sn	1.3	2.59	0.0059	6.4
SnMNa/523	Mn–O, or C	3.4	1.94	0.0131	8.5
	Mn–Mn	1.0	2.37	0.0029	–1.9
	Mn–Mn	0.6	3.00	–0.0022	0.5
	Mn–Mn	1.0	3.31	–0.0021	–0.7
	Mn–Mn	1.2	3.68	0.0000	–0.3
	$Me_3SnMn(CO)_5$ in H_6Y				
SnMH6RT	Mn–CO	5.2	1.87	0.0028	0.3
	Mn–*C*O	6.0	2.98	–0.0037	1.9
SnMH6/373	Mn–CO	4.9	1.84	0.0015	1.5
	Mn–*C*O	6.4	2.97	–0.0033	1.6
SnMH6/423	different Mn–Mn distances between about 2.4 and 3.7 Å				
SnMH6/523	Mn–O	3.4	2.21	0.0007	0.8
	Mn–Si	4.7	3.37	0.0019	–1.8

[a] Coordination number. [b] Bond distance. [c] Static disorder. [d] Inner potential. [e] Fit result obtained when Mn–Sn was included in second shell fit.

The above precursor was immobilized into three types of zeolite Y containing different proton concentrations. NaY (commercial Linde LZ-Y52 $[Na_{57}Al_{57}Si_{135}O_{384}]\cdot 235H_2O$), highly acidic H6Y (6 H$^+$/sc) from Linde LZ-Y62 $[(NH_4)_{45}Na_{10}Al_{55}Si_{137}O_{384}]\cdot 235$ H_2O, and H2Y (2 H$^+$/supercage, sc), derived from ammonium-exchanged NaY, were used. Heating the ammonium-exchanged zeolite under oxygen flow at 100 °C for 4 h and at 450 °C for 10 h, then under vacuum at the same temperature for 5 h (at a rate of 1 °C/min) resulted in the desired acid form. The dehydrated zeolites were kept in sealed vials in a glovebox prior to further treatments. An amount of 0.500 g of each zeolite was loaded with one molecule/supercage of $Me_3SnMn(CO)_5$ in 50 mL of hexane by stirring the slurry for 12 h under dry nitrogen

TABLE III: EXAFS Data Derived from the Sn Edge

sample	atom pair	N^a	R/Å^b	$\Delta\sigma^2$/Å^{2,c}	ΔE/eV^d
		$Me_3SnMn(CO)_5$ Precursor			
SnM	Sn–Me	3.0	2.11	0.0035	−0.7
		$Me_3SnMn(CO)_5$ in NaY			
SnMNa/RT	Sn–Me	0.9	1.97	0.0049	2.8
	Sn–Me	1.9	2.14	−0.0007	−1.5
	Sn–Mn	1.2	2.72	−0.0008	−1.7
SnMNa/423	Sn–Me	2.7	2.10	0.0041	−3.4
	Sn–Mn	1.3	2.60	−0.0014	−0.5
SnMNa/523	Sn–Sn	2.2	1.94	−0.0014	−5.7
	Sn–Sn	0.5	2.10	−0.0054	6.8
		$Me_3SnMn(CO)_5$ in H6Y			
SnMH6/RT	Sn–O_1/Me_2[e]	2.4	2.13	0.0011	−2.2
	Sn–Mn	1.2	2.56	−0.0013	2.9
SnMH6/373	Sn–O_2/Me_1[e]	2.6	2.11	0.0008	−1.4
	Sn–Mn	0.9	2.58	−0.0019	−2.3
SnMH6/393	Sn–O_2/Me_1[e]	2.7	2.11	0.0012	−2.1
	Sn–Mn	0.5	2.58	−0.0052	0.6
SnMH6/423	Sn–Me[f]	0.9	1.95	0.0018	−4.3
	Sn–O	2.8	2.15	0.0032	1.4
SnMH6/523	Sn–Me[f]	1.0	1.91	−0.0003	−1.7
	Sn–O	3.0	2.12	0.0003	1.8
	Sn–Mn/Si	nd[g]			

[a] Coordination number. [b] Bond distance. [c] Static disorder. [d] Inner potential. [e] The relative O_x/Me population at Sn is derived from the IR data. [f] The shorter bond is assigned to Sn–Me because only one Me is left. [g] nd = not determined.

atmosphere. The slurry was filtered and washed several times with hexane. The intrazeolite samples were dried by a mechanical vacuum pump. The IR data of the filtrates of all samples show the presence of a residual amount of the precursor in the solvent. AAS data indicate an average actual loading of 0.5 $Me_3SnMn(CO)_5$ molecules/sc. The low loading level was chosen so that even a potential local attack at the framework would not lead to zeolite disintegration.

EXAFS samples for thermal stability studies were prepared by heating the 0.500-g batches of zeolites in a tube furnace at 323, 353, 373, 393, and 523 K under 10^{-5} Torr vacuum. The temperature was ramped up at a heating rate of 1 K/min to the desired temperature and kept constant for 10 h. The treated samples were transferred under vacuum to the dry nitrogen box. The powdered samples were mixed with a molten, degassed 1:1 mixture of octadecane and eicosane at 303–308 K, and the encapsulated samples were packaged in EXAFS sample holders, sealed with Kapton tape and kept under nitrogen until EXAFS measurements were performed.

Characterization. FTIR data were taken with a Mattson Polaris spectrometer at 4-cm^{-1} resolution. NMR measurements were carried out using a Bruker 250 spectrometer. The lock solvent for NMR measurements was $CDCl_3$. Mass spectra of the precursor and the NaY sample were taken on a Finnigan 4500 series mass spectrometer under high vacuum (10^{-7} Torr) with a heating rate of 30 K/min from 323–573 K, in the mass range 12–800 amu, and electron energy of 30 eV.

In Situ FTIR-TPD-MS. FTIR data were taken with a Mattson Polaris spectrometer at 4-cm^{-1} resolution. Each sample was prepared as a thin dispersion on a Si wafer and introduced into a steel cell with CaF_2 windows under nitrogen atmosphere in a glovebox. The cell was connected to a turbomolecular pump combined with a quadrupole mass spectrometer (Dycor M200, 1–200 amu). Prepumping was achieved with molecular sieve pumps in order to eliminate hydrocarbon contamination. The residual H_2 pressure did not interfere with the measurements. The sample was evacuated until the total pressure (including H_2) was $<10^{-5}$ Torr prior to any treatment. Up to 5 mass fragments could be monitored as a function of time/temperature in the TPD-MS experiment. Zeolite samples were heated at 1 K/min up to 573 K while the FTIR and mass spectra were continuously monitored.

EXAFS measurements were carried out at NSLS (Brookhaven National Laboratories) at beamline X-11A with a stored energy of 2.5 GeV and ring currents between 90 and 180 mA. The data were collected at the Mn K-edge (6329 eV) and the Sn K-edge (29 200 eV) of the $Me_3SnMn(CO)_5$ samples. The experiments were performed at about 100 K in transmission using a double crystal Si(400) monochromator. Sample notations are assigned as follows: SnM represents trimethyltin manganese pentacarbonyl. Na, H2, and H6 correspond to the types of zeolite Y supports by omitting the symbol Y. Abbreviated treatment temperatures are included in the suffix of the sample name; e.g., SnMNa/RT relates to $Me_3SnMn(CO)_5$ in NaY at room temperature. SnMH6/393 relates to $Me_3SnMn(CO)_5$ in H6Y heated to 393 K under vacuum. The EXAFS data were analyzed using standard procedures, as described in a previous article[16c] and in the supplementary material (see paragraph at end of paper). Crystallographic data of the reference compounds used for the EXAFS data analysis are listed in Table I.

Results and Discussion

$Me_3SnMn(CO)_5$ in NaY. (*a*) *Mn Absorption Edge.* The k^2-weighted Fourier transforms of the complex $Me_3SnMn(CO)_5$ in NaY at room temperature, 423 and 523 K are shown in Figure 2A–C. In comparison with the FT of the precursor (Figure 1A), the Mn–Sn shell in the middle seems to have vanished after the precursor was loaded into NaY (Figure 2A). However, the oxygen shell peaking at 2.5 Å appears much more intense than the carbon shell at 1–1.8 Å. This is due to an overlap between oxygen and tin contributions in the second shell, as discussed below. The fit result for the carbon shell shows 4.3 carbon atoms at a distance of 1.83 Å from the Mn center (Table II). The second shell (k^2, 1.72–2.74 Å) was back filtered and fitted with the Mn–C*O* reference shell from $Mn(CO)_5$. Six oxygen atoms were found at 2.97 Å. This high number implies coordination to Sn in the second shell, but this contribution could not be determined precisely.

The FT function of the same sample heated at 393 K is not significantly different, but at 423 K, the Mn–Sn shell becomes visible (with an enlarged *y* axis) at about 2.1 Å due to the disappearance of the CO shells. At 523 K, the appearance of several Mn–Mn shells indicates formation of Mn clusters.

(*b*) *Sn Absorption Edge.* The Fourier transforms of Sn edge data of the NaY samples are shown in Figure 2D–F. When the precursor is introduced into NaY, the first shell splits into two peaks. Since no reactive species are present in NaY, this effect should be due to two different Sn–C distances. The second shell is very similar to that observed for the precursor itself. Two distances of Sn–C were, indeed, found at 1.97 and 2.14 Å with coordination number 0.9 and 1.9, respectively. The Sn–Mn bond is longer than in the precursor: N = 1.2 atoms, R = 2.72 Å. This may be due to the effect of intrazeolite Na^+ on increasing the π-backbonding from Mn to CO ligands and resulting in less d interaction in the Sn–Mn bond.

At higher temperatures up to 423 K, no significant change in coordination number for both Sn–C and Sn–Mn is observed. At 423 K, the Sn–C and Sn–Mn peaks become broader and overlap each other. A two-shell fit shows 2.7 carbon atoms at 2.10 Å and 1.3 manganese atoms at 2.60 Å, respectively. The Sn–Mn distance is similar to that obtained from the Mn absorption edge (2.59 Å). Drastic changes occur at 523 K. The Sn–Mn bond is cleaved and new Sn species are formed. A fit with Sn foil shows N = 2.2 atoms at 1.94 Å and N = 0.5 atoms at 2.10 Å, respectively, but these distances are far shorter than in bulk tin (3.02 Å in white tin). They are also too short for Sn–Mn alloys.[20] At this point, these results cannot be explained with the potential tin species that could be present in the zeolite.

The EXAFS results discussed above show that the NaY host does not cause methyl substitution at the Sn atom in $Me_3SnMn(CO)_5$. The precursor appears to remain intact in the NaY pore system up to 393 K. All carbonyl ligands are split off at 423 K while the Sn–Mn and Sn–Me bonds are still stable. The loss of CO ligands occurs between 393 and 423 K, which is comparable to the decomposition range of the unsupported precursor. Heating the precursor itself in a sealed tube at 403 K in

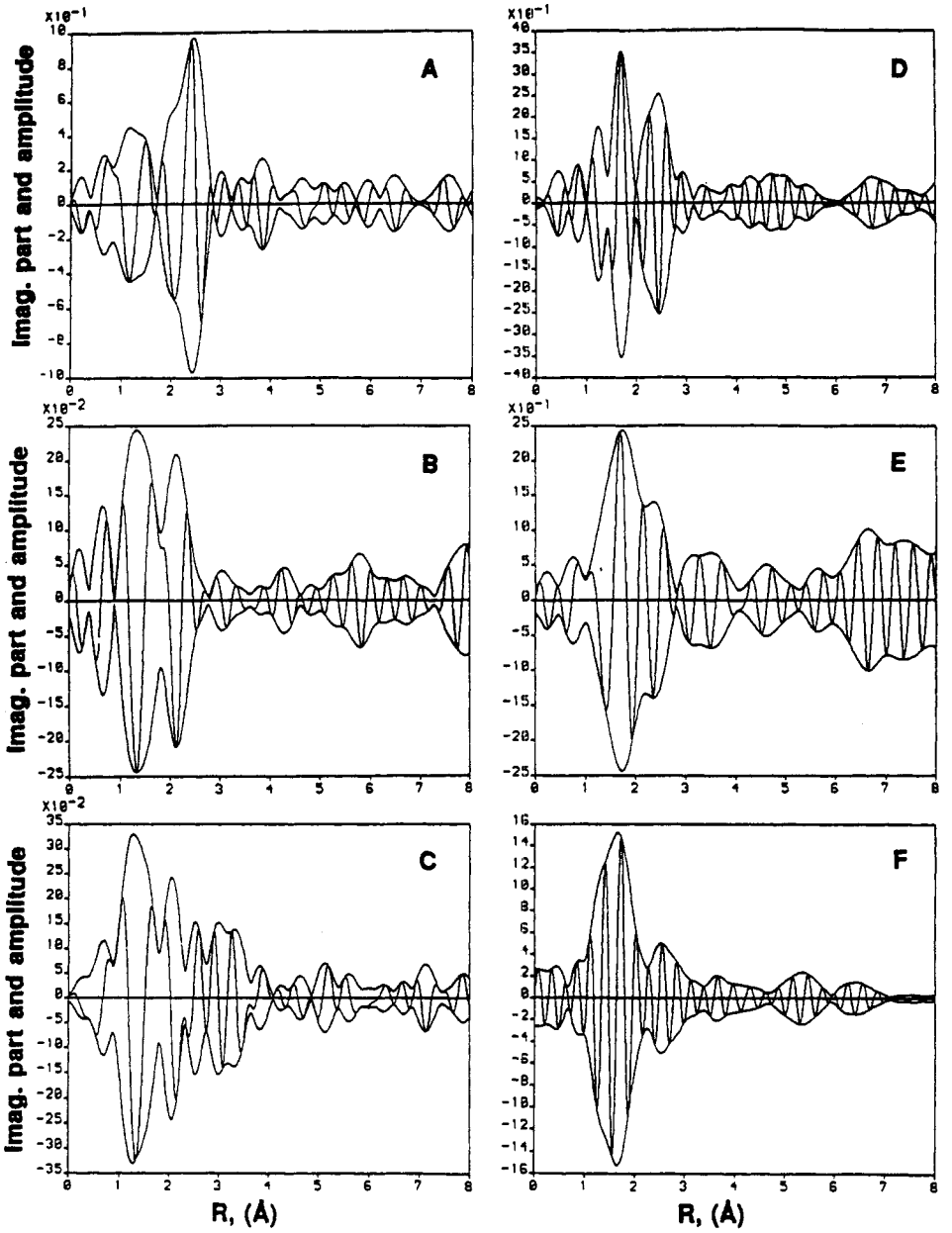

Figure 2. FT of EXAFS samples. $Me_3SnMn(CO)_5$ in NaY, Mn edge spectra: (A) at RT, FT = k^2, 3.2–10 Å^{-1}. (B) At 423 K, FT = k^2, 2.7–10 Å^{-1}. (C) At 523 K, FT = k^2, 2.7–11 Å^{-1}; Sn edge spectra: (D) At RT, FT = k^3, 2.7–12 Å^{-1}. (E) At 423 K, FT = k^3, 2.7–10 Å^{-1}. (F) At 523 K, FT = k^3, 2.6–12 Å^{-1}.

the dark for 48 h did not show a significant change (97.6% recovery).[21] After the loss of CO ligands, it is likely that the Mn atom associates with zeolite oxygen atoms. The fit results show coordination of Mn to 2.7 oxygen atoms while the Mn–Sn and Sn–Me_3 coordination remains unchanged. At 523 K, in addition to Mn–Oz (Oz = oxygen atoms in the zeolite framework) or Mn–C bonds (N = 3.4 atoms, R = 1.94 Å), several of the Mn–Mn bond distances observed (2.37–3.68 Å) are in the range known for bulk α-Mn and several Mn compounds.[22]

In Situ FTIR-TPD-MS Results. The IR spectra of $Me_3SnMn(CO)_5$ in NaY treated under vacuum at room temperature, 373, 443, 473, and 523 K are shown in Figure 3. At room temperature, the carbonyl region shows six bands at 2098, 2082 (sh), 2034, 2007, 1969, and 1952 cm^{-1}. On the basis of their behavior with increasing temperature, these bands are assigned to weakly adsorbed species at 2098, 2034, and 1969 cm^{-1} and strongly adsorbed species that interact with the Na ions: 2082 (sh), 2007, and 1952 cm^{-1}. In nonpolar solvents, only three carbonyl bands are expected for a C_{4v} moiety. In the zeolite, the interaction between Na^+ ions and oxygen on CO ligands can cause the lowering of molecular symmetry.[6] Upon heating, the band intensities of the physically adsorbed species decrease slowly while the strongly adsorbed species is unaffected even at 373 K. The intensity of the band at 2080 cm^{-1} increases at 383 K, while the rest of the group decreases. This may be due to a change in symmetry after the weakly adsorbed complex has left the zeolite cages. At the same time, a new peak appears at 2106 cm^{-1} that becomes more visible at 403 K. The intensities of the band at 2080 cm^{-1} and the new peak reach a maximum at 443 K and decrease above 453 K.

It should be noted that the temperatures of the in situ thin-layer experiments may not be compared directly to the temperatures of EXAFS batch experiments. We have found that reactions in batch geometry are far slower than in the thin dispersions in high vacuum, probably due to the much lower gas partial pressures at the zeolite crystal surface in the latter experiments. Desorption mass spectra of $Me_3SnMn(CO)_5$ in NaY were measured at a fast heating rate of 30 K/min. The desorption temperatures are comparable to the FTIR conditions due to the small sample mass. Figure 4B shows that significant desorption of several masses (CH_4, CO) is observed at 453 K with a maximum at 495 K. Figure 4A shows the mass bar pattern detected at 495 K with carbon monoxide (mass 28) as the most intense peak. Similar to the mass fragmentation of the precursor, no Sn or $Mn(CO)_n$

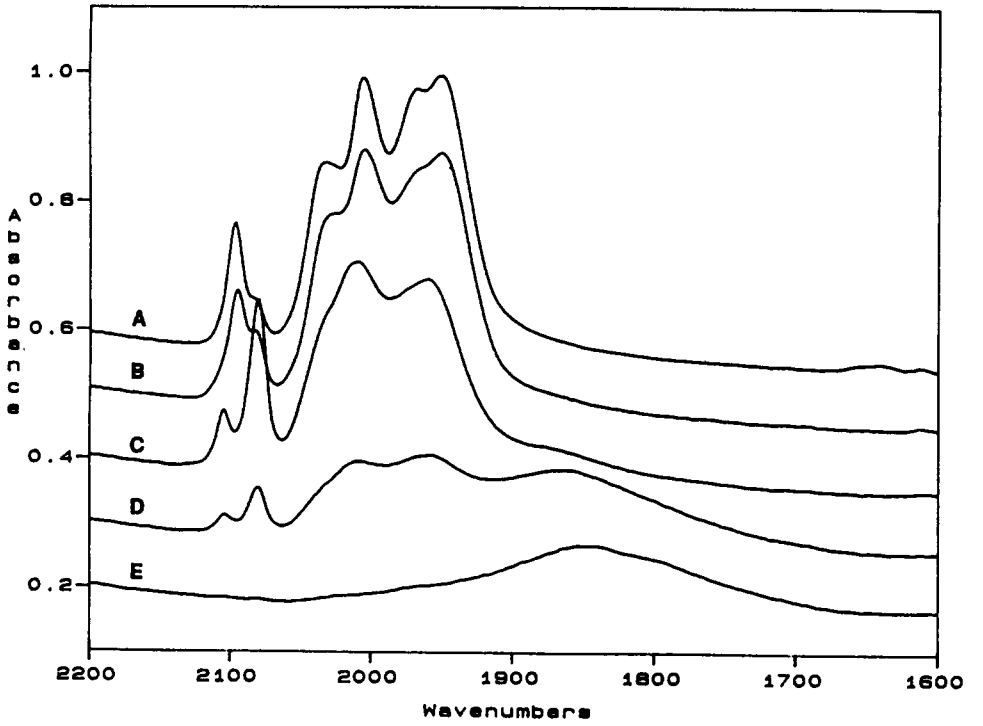

Figure 3. CO stretching vibrations (in situ FTIR measurements) of $Me_3SnMn(CO)_5$ in NaY: (A) RT, vacuum; (B) 373 K; (C) 443 K; (D) 473 K; (E) 523 K.

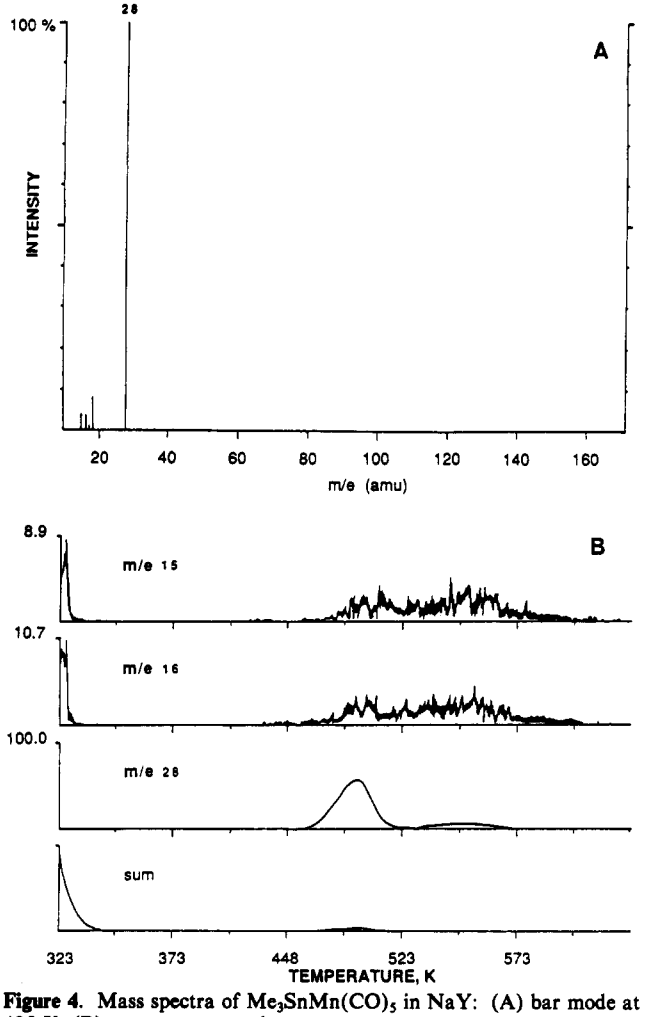

Figure 4. Mass spectra of $Me_3SnMn(CO)_5$ in NaY: (A) bar mode at 495 K; (B) temperature mode.

(n = 1–5) fragments were found, neither was the Mn fragment (mass 55). (The precursor mass spectrum contains the Mn fragment.) Thus, the strongly adsorbed $Me_3SnMn(CO)_5$ species

SCHEME I: Chemistry of $Me_3SnMn(CO)_5$ in NaY Zeolite

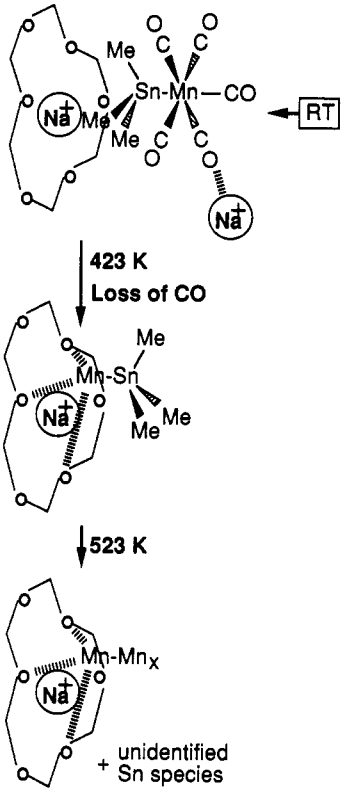

identified in the FTIR experiments decomposes at about 453 K by loss of CO and CH_3 ligands with a maximum desorption at 495 K. Mn and Sn remain inside the zeolite and form new intrazeolite metal species.

The interpretation of the reaction pathways of $Me_3SnMn(CO)_5$ in the NaY host is summarized in Scheme I.

$Me_3SnMn(CO)_5$ in H6Y. *Mn Absorption Edge.* The EXAFS data of H6Y samples are shown in Figure 5A–D, and data analysis results are presented in Table II. At room temperature (Figure 5A), the transform at the Mn edge is similar to that in NaY. A full carbonyl coordination shell was found: 5.2 carbon atoms at

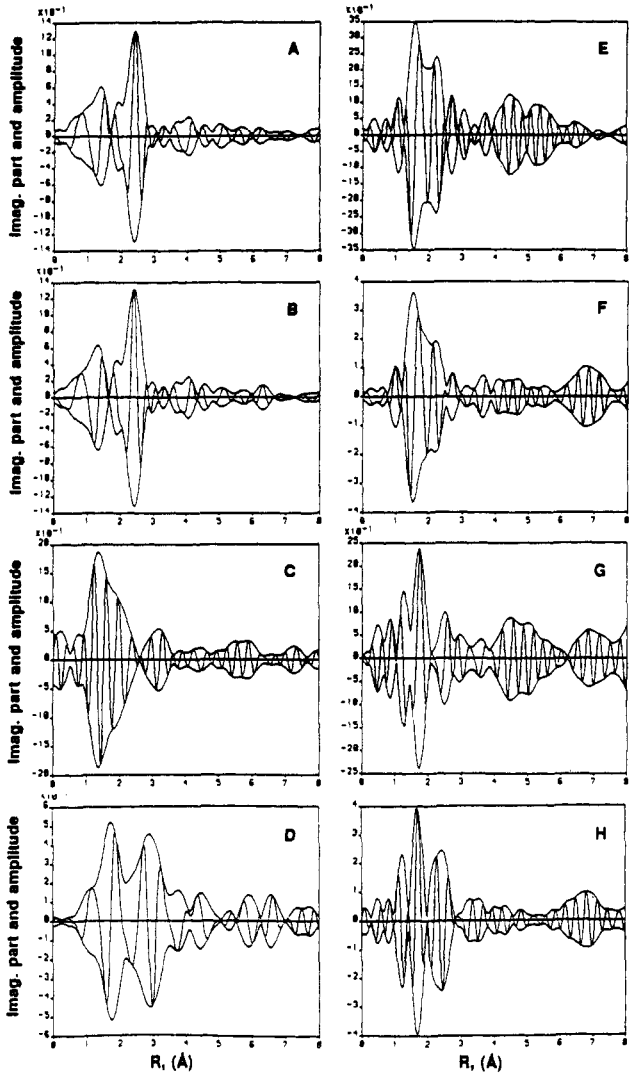

Figure 5. FT of EXAFS samples. $Me_3SnMn(CO)_5$ in H6Y: Mn edge: (A) at RT, FT = k^2, 3.1–11 Å^{-1}; (B) at 373 K, FT = k^2, 3.2–12 Å^{-1}; (C) at 423 K, FT = k^2, 2.5–11 Å^{-1}; (D) at 523 K, FT = k^2, 2.5–11 Å^{-1}; Sn edge: (E) at RT, FT = k^3, 2.6–12 Å^{-1}; (F) at 373 K, FT = k^3, 2.5–12 Å^{-1}; (G) = at 423 K; FT = k^3, 2.7–12 Å^{-1}; (H) at 523 K, FT = k^3, 2.7–12 Å^{-1}.

1.87 Å and 6.0 oxygen atoms (Sn backscattering included) at 2.98 Å. At 373 K (Figure 5B), the carbonyl coordination remains stable with 4.9 carbon atoms and 6.4 oxygen atoms (Sn modulation included) at 1.84 and 2.97 Å, respectively. At 423 K (Figure 5C), dramatic changes in the FT are observed. The carbon and oxygen shells of the CO ligands have disappeared. Because the corresponding χ functions show the k dependence typical for the Mn backscattering, the EXAFS data indicate the formation of small Mn clusters with Mn–Mn distances between about 2.4 and 3.7 Å. Due to the substantial overlap of the shells, a detailed analysis was not attempted. At 523 K (Figure 5D), the Fourier transform presents a Mn–O bond as a first shell (N = 3.4 atoms, and R = 2.21 Å) and Mn–Si as an outer shell (N = 4.7 atoms, and R = 3.37 Å using the Mn–S shell as a reference). The two shells of the sample at 523 K in Figure 6 show the excellent quality of the fits.

Sn Absorption Edge. The tin EXAFS data of the precursor in H6Y are shown in Figure 5E–H and Table III. Fit results of the data stripped of the Sn–Si shell show 2.4 atoms of C or O at 2.13 Å and the Sn–Mn bond at 2.56 Å (N = 1.2 atoms). The Sn–Mn bond length shrinks significantly compared to the Sn–Mn bond of the precursor. This effect was also found for the Sn–Mn bond (average distance = 2.59 Å) in $Cl_3SnMn(CO)_5$.[23] Most likely, the replacement of methyl groups by electronegative ligands increases electron density for the Sn–Mn π interaction by decreasing π back-bonding in the Mn–C bonds. This is also suggested by the elongated Mn–CO distance in this sample (1.83 Å in NaY versus 1.87 Å in H6Y at room temperature).

At 373 K, no drastic changes were observed, but at 423 K, the Sn–Mn shell disappears and the outer Si shell is now clearly visible (Figure 5G). The back-filtered outer peak shows that this shell is due to Si and not to Mn. The Sn–Mn bond is thus cleaved at this temperature, and the resulting tin species must remain attached to the zeolite framework. The first tin shell of the 423 K sample is split into two contributions with a total coordination number of about 4, which both represent oxygen/carbon backscattering (Table III). Structural data of the unsupported $Me_3SnMn(CO)_5$ show one short (2.06 Å) and two long Sn–Me bonds (2.16 Å).[24] The zeolite alone cannot offer more than 3 oxygen atoms per 6-ring. Due to the previous removal of most methyl ligands, the one ligand is assigned to Sn–Me (N = 0.9) and the three ligands at 2.15 to the Sn–O_z coordination where O_z are the oxygen atoms of the 6-ring of the acid zeolite. The incomplete substitution of the methyl ligands of the precursor $Me_3SnMn(CO)_5$ in H6Y is in agreement with the studies in solution: A maximum of two methyl groups of $Me_3SnMn(CO)_5$ could be substituted by chloride from gaseous HCl.[17]

At 523 K (Figure 5H), the coordination to the methyl and O_z ligands is found again (1.91 Å and 2.12 Å). The outermost shell is due to metal backscattering.

FTIR-TPD-MS Results. The IR spectra of the $Me_3SnMn(CO)_5$ precursor in H6Y are shown in Figure 7. The IR pattern at room temperature appears to be based on two species: 2136, 2055, and 2024 cm^{-1} and 2115, 2024 and 1992 cm^{-1}. The latter group is assigned to singly substituted $(O_z)Me_2SnMn(CO)_5$, O_z = zeolite oxygen framework. The former group is associated with doubly substituted $(O_z)_2MeSnMn(CO)_5$. The shift to higher frequency with increasing substitution indicates the replacement of methyl groups by electronegative atoms, i.e., oxygen of the

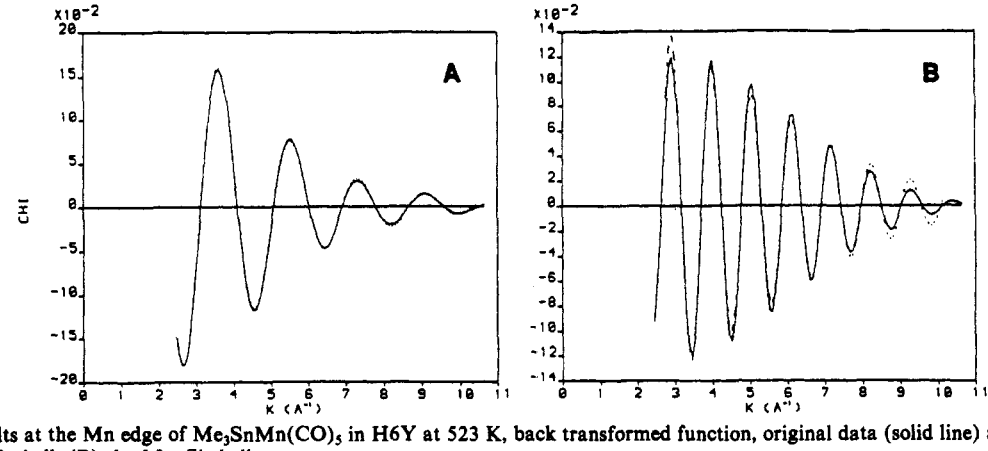

Figure 6. Fit results at the Mn edge of $Me_3SnMn(CO)_5$ in H6Y at 523 K, back transformed function, original data (solid line) and fit (dashed line) of: (A) the Mn–O shell; (B) the Mn–Si shell.

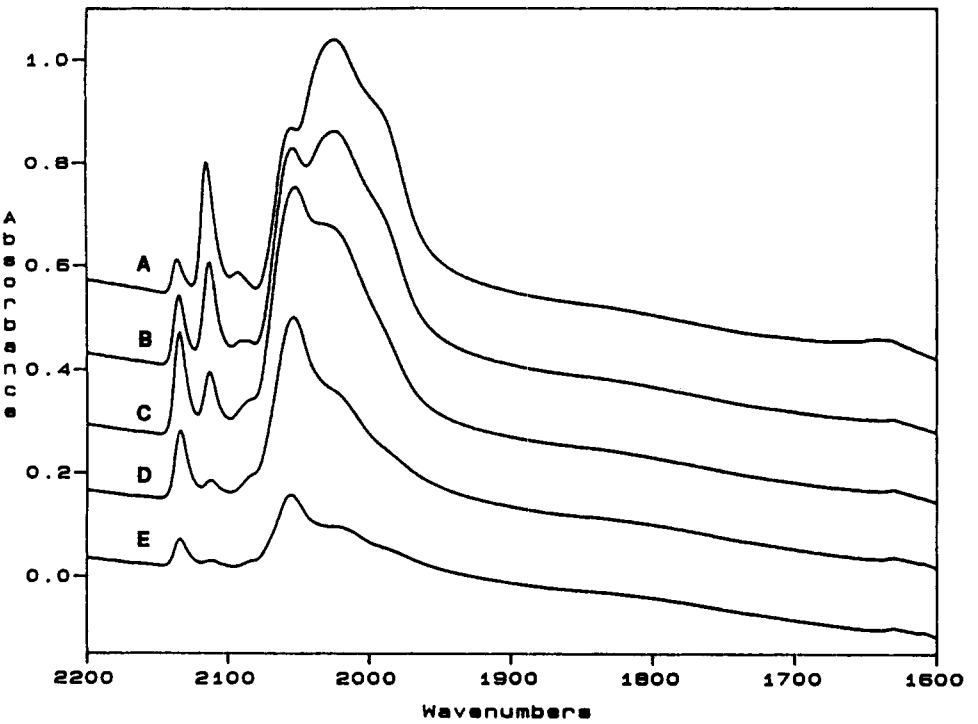

Figure 7. CO stretching vibrations (in situ FTIR measurements) of $Me_3SnMn(CO)_5$ in H6Y: (A) RT, vacuum; (B) 343 K; (C) 373 K; (D) 403 K; (E) 423 K.

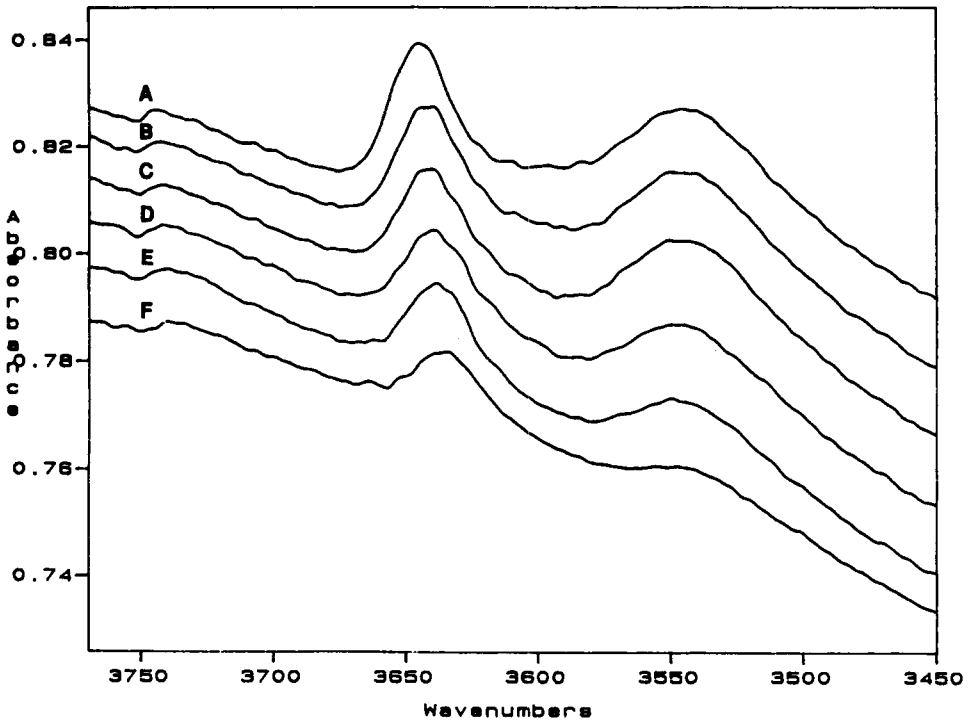

Figure 8. OH stretching vibrations (in situ FTIR measurements) of the zeolite host with sample $Me_3SnMn(CO)_5$ in H6Y, (A) RT, vacuum; (B) 343 K; (C) 373 K; (D) 403 K; (E) 423 K; (F) 543 K.

zeolite framework, and is consistent with reduced Mn–CO π-backbonding as discussed above. Similar frequency shifts were also observed between $Cl(Me)_2SnMn(CO)_5$ (2101, 2015, and 2006 cm^{-1}, in cyclohexane[25]) and $Cl_3SnMn(CO)_5$ (2126, 2046, and 2040 cm^{-1} in hexane[26]). Upon heating the zeolite sample at 343 K, the intensity of the higher frequency group (double substitution, 2136, 2055, and 2024 cm^{-1}) increases with a concomitant decrease in the intensity of the lower frequency group (2115, 2024, and 1992 cm^{-1}). This accounts for the transformation of the mono-substituted into the disubstituted species. The concentration of the disubstituted species reaches a maximum at 373 K (Figure 7C) and decreases at higher temperatures.

At elevated temperature, a decrease of *both* the supercage hydroxyl and the sodalite hydroxyl band at about 3550 cm^{-1} was observed (Figure 8). The latter effect indicates migration of protons from the sodalite cages to react with the organometallic species in the supercages, and explains the higher degree of substitution of methyl groups by zeolite framework oxygen at higher temperatures.

During the in situ IR measurements, the evolved gases were monitored with a mass spectrometer. The results are shown in Figure 9. Methane (mass 16; A) begins to desorb at 328 K with three maxima at 349, 403, and 471 K, respectively. Concomitant with the first, most intense maximum, desorption of CO (mass

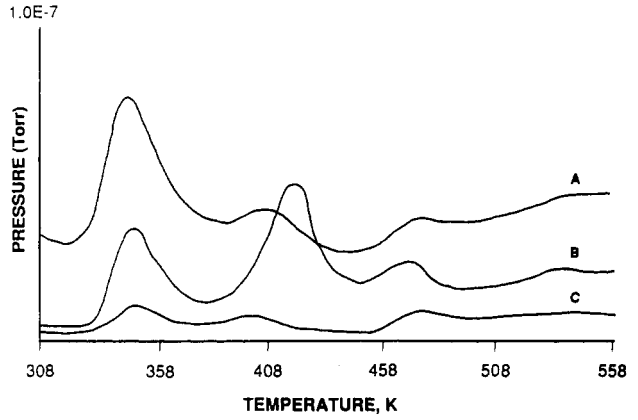

Figure 9. TPD-MS spectra of $Me_3SnMn(CO)_5$ in H6Y: (A) CH_4 (mass = 16); (B) CO (mass = 28); (C) Mn (mass = 55), measured simultaneously with the FTIR spectra in Figures 12 and 13.

28) and Mn (mass 55) also appears in the TPD profile. The first desorption is assigned to volatile residual precursor which may be obscured by the broad IR bands of the attached species. The small peak at 2095 cm^{-1} could be indicative of physisorbed complex, as in the NaY host (see above). It seems that some fraction of the monosubstituted species $(O_z)Me_2SnMn(CO)_5$ decomposes during the transformation to disubstituted species $(O_z)_2MeSnMn(CO)_5$ and generates the CO and Mn fragments in the TPD/MS profile. The second desorption at about 403 K is associated with the decomposition of the disubstituted species. Desorption of CO (mass 28) and Mn (mass 55) also appeared in the TPD profile at the same time as the second desorption of CH_4, but tin fragments were not observed. This indicates that the tin species are held within the zeolite cages. In addition, CO, Mn, and Sn (mass 119) fragments were observed along with the third desorption of CH_4 peaking at 471 K, indicating fragmentation of the intrazeolite subcarbonyl species formed by the decomposition of the substituted species.

From combined EXAFS, FTIR, and TPD-MS results of $Me_3SnMn(CO)_5$ in H6Y, conclusions can be drawn as shown in Scheme II. Already at room temperature, the compound attaches to the zeolite framework at the oxygen rings of the supercage. The attachment of the molecule occurs through the Sn moiety by loss of CH_4 gas while the Sn–Mn bond and the CO ligand sphere are still intact. The substitution of methyl ligands by oxygen atoms of the zeolite framework is supported by the EXAFS results which indicate that the electronegative oxygen atoms increase the Sn–Mn bond strength of the attached precursor in H6Y zeolite. This inductive effect of oxygen may influence the $d\pi$–$d\pi$ interaction between the Sn and Mn atoms by withdrawing π-electrons through the Sn–Mn–CO system (resulting also in a decrease of π-backbonding in the Mn–CO bonds). The weakened Mn–CO interaction is also confirmed by the higher CO-stretching frequencies of the precursor in H6Y. On the basis of the IR data, both mono- and disubstitution of methyl groups by the framework oxygen atoms occurs. The monosubstituted species, (O_z)-$Me_2SnMn(CO)_5$, is the major product at room temperature while the disubstituted species, $(O_z)_2MeSnMn(CO)_5$, is formed at higher temperature, ca. 373 K. The attached species decompose at 423 K by loss of CO ligands and cleavage of the Sn–Mn bond. As discussed above in the EXAFS section, one methyl ligand remains on the zeolite-attached tin atom. Unidentified Mn species are left inside the zeolite cavities as a result of the decomposition. At 523 K, both Mn and Sn species are attached to the zeolite framework.

$Me_3SnMn(CO)_5$ in H2Y. *EXAFS Results.* The EXAFS spectrum of the precursor in the partially proton-exchanged H2Y at room temperature is comparable to that in H6Y. The results at the Mn edge show 4.5 carbon atoms at a distance of 1.84 Å and 6.9 oxygen atoms (including the Sn contribution) at 2.97 Å. At the Sn edge, 2.4 oxygen/carbon atoms at 2.16 Å and 0.7 Mn atoms at 2.60 Å were found.

FTIR-TPD-MS Results. The IR spectra for in situ experiments are shown in Figure 10. The intrazeolite chemistry in H2Y is intermediate between H6Y and NaY. Only the low-frequency carbonyl species assigned to mono-substitution was found as a product (2114, 2023, and 2000 cm^{-1}). The hydroxyl stretch of the zeolite framework was not observed even at room temperature. This indicates the consumption of all available zeolite protons in the reaction of H2Y with $Me_3SnMn(CO)_5$. Considering the proton/complex stoichiometry, there are probably not enough protons in H2Y to substitute more than one methyl group per complex. The remaining Na^+ ions interact with the unreacted precursor (2099, 2023, and 1959 cm^{-1}) as in NaY. Loss of CO

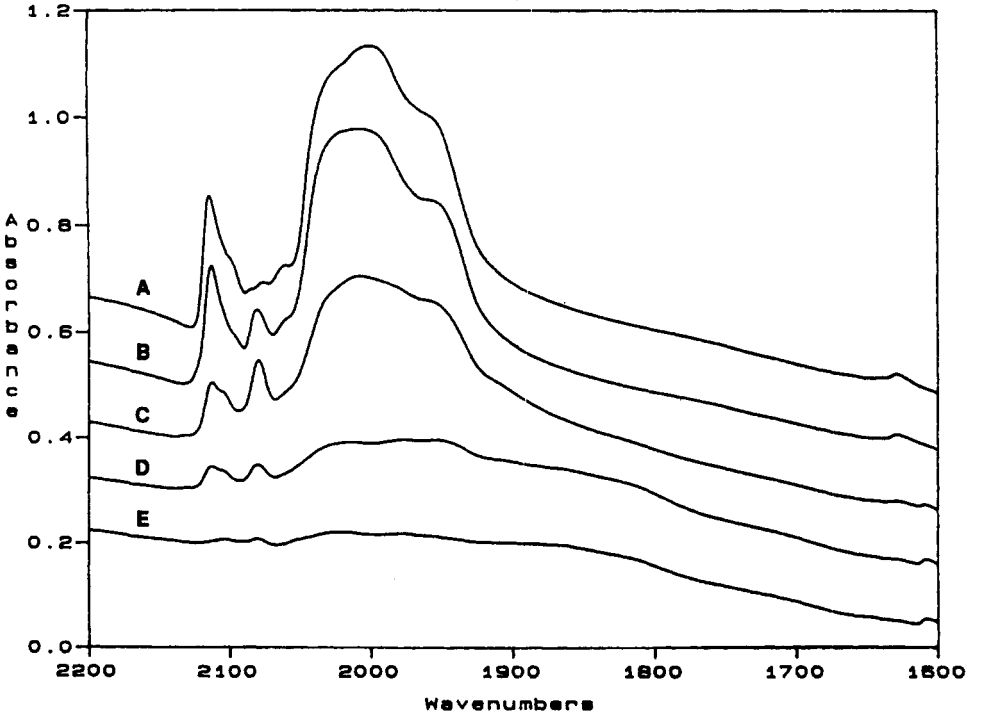

Figure 10. CO stretching vibrations (in situ FTIR measurements) of $Me_3SnMn(CO)_5$ in H2Y, (A) RT, vacuum; (B) 373 K; (C) 433 K; (D) 473 K; (E) 543 K.

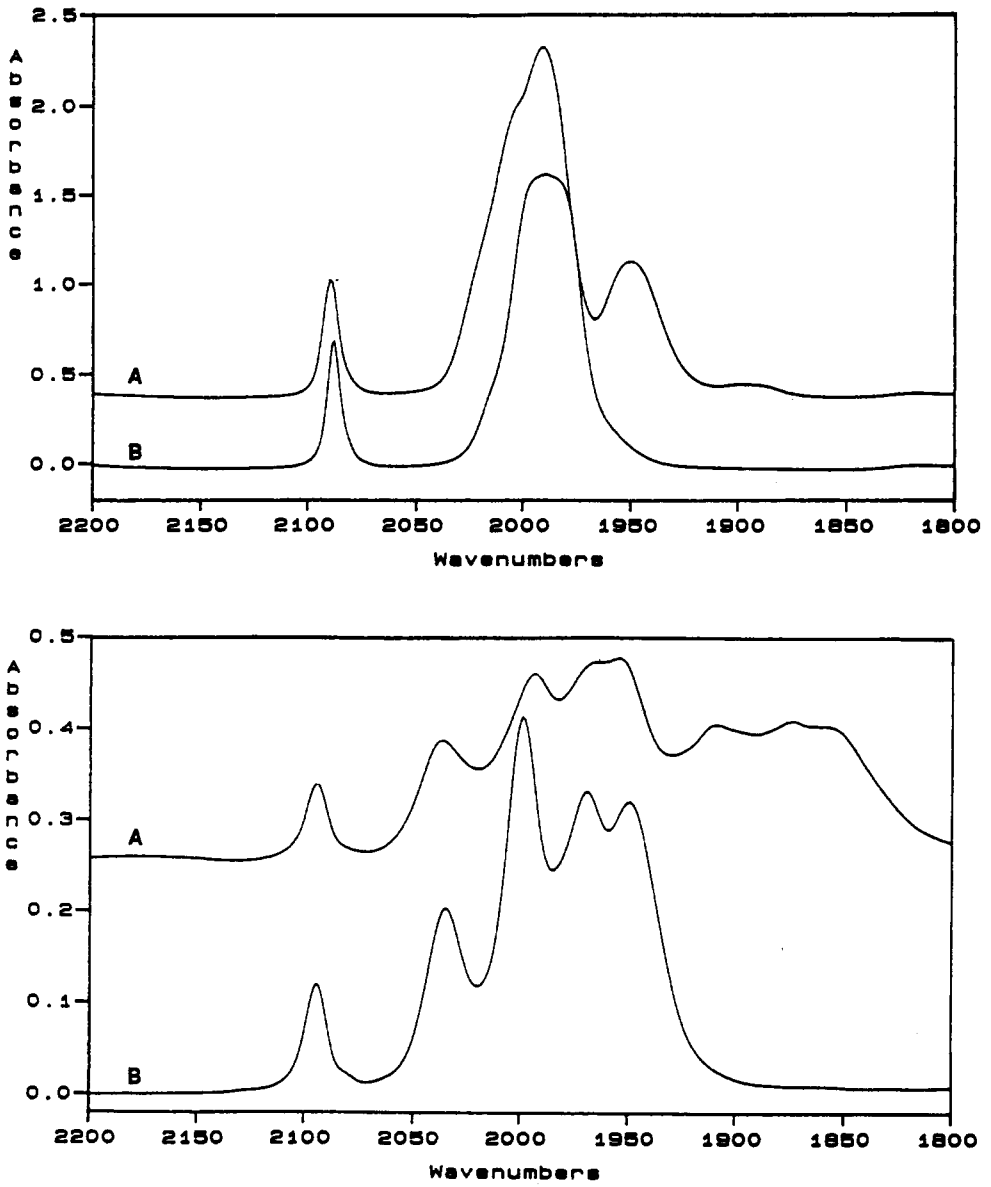

Figure 11. IR spectra of $Me_3SnMn(CO)_5$ treated with PEt_3 at 1:1 molar ratio: (top) precursor, in $CDCl_3$ and (bottom) in NaY, Nujol mulls (A) before and (B) after the treatment.

ligands at higher temperature results in the shift of the remaining CO bands to lower frequencies.

Reactivity of Intrazeolite Compounds. A reaction of the non-thermally-treated complex species in NaY with PEt_3 was studied in comparison to the reactivity of the unsupported precursor in solution. The reaction was carried out under nitrogen at room temperature by stirring 1:1 molar ratios of the reactants for 10 h in hexane.

Reactivity of the Unsupported Precursor. The characterization of the reaction products in solution was performed without an attempt of product separation. $CDCl_3$ was used as a solvent for the solution reactions. The $CHCl_3$ impurity in $CDCl_3$ was used as a standard peak position for ^1H NMR, and H_3PO_4 was used as reference for ^{31}P NMR studies. With $P(OMe)_3$, no color change was observed for the solution reaction of the unsupported precursor. ^{31}P NMR data showed no reaction of the precursor with the $P(OMe)_3$ ligand. Only the characteristic resonance of free $P(OMe)_3$ (δ_P = 141 ppm) was found in the solution. ^1H NMR data showed also no change of the CH_3–Sn resonance (δ_{Me} = 0.46 ppm). However, during the overnight reaction with PEt_3, the color of the solution changed from colorless to yellow. No free PEt_3 (δ_P = −18 ppm, δ_H = 0.58 (CH_2) and 0.24 (CH_3) ppm, this work) was detected by ^1H and ^{31}P NMR. A new ^{31}P resonance was found downfield, i.e., δ_P = 31.4 ppm. This is not $OPEt_3$, which was reported to be at δ_P = 48 ppm.[27] ^1H NMR data showed the undisturbed chemical shift of CH_3–Sn. The new bands at 2005, 1950, and 1890 cm^{-1} in the CO stretching pattern (Figure 11, top) result from the reaction with PEt_3. The number of bands is consistent with a *cis*-$LMn(CO)_4(PEt_3)$ carbonyl complex. The observation of CO bands at lower frequencies confirms CO substitution by the phosphine with the associated increase in electron back bonding from Mn to the remaining CO ligands. Some of the free precursor complex did not react, as indicated by small remaining band intensities at 2090 and 1991 cm^{-1}.

Reactivity of the Precursor in NaY. The reaction of the precursor in NaY with PEt_3 was carried out in *n*-hexane. After a reaction period of 10 h, the zeolite sample was filtered and the unreacted PEt_3 ligand was washed off by using *n*-hexane. The IR spectra of the zeolite samples were measured as Nujol mulls. The IR data of the sample in NaY treated with PEt_3 (Figure 11, bottom) show a shift to lower frequency similar to the solution reaction. The new bands at 1909, 1873, and 1860 cm^{-1} are lower than those of the substitution product in solution, probably due to the effect of Na^+ ions in NaY. These observations demonstrate that the intrazeolite complex $Me_3SnMe(CO)_5$ can react with a phosphine ligand that diffuses into the pore system from solution.

Conclusions

The combination of EXAFS data and in situ FTIR coupled with TPD-MS measurements discussed above provides a com-

SCHEME II: Chemistry of $Me_3SnMn(CO)_5$ in H6Y Zeolite

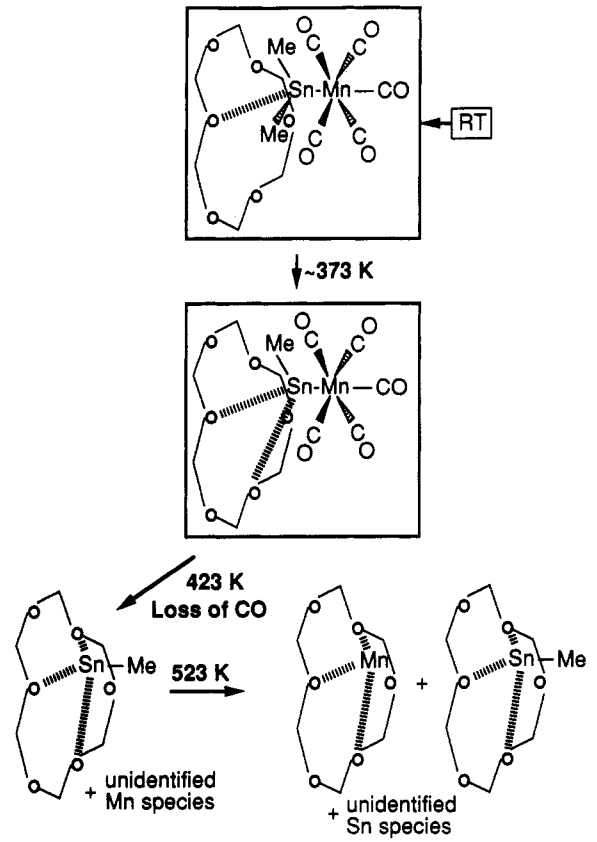

prehensive picture of the intrazeolite structure and chemistry of $Me_3SnMn(CO)_5$. The thermal stability of the Sn–Mn and the Mn–CO bonds of the precursor in the zeolite hosts is very similar to that of the free complex.

In the "neutral" environment of the NaY host, the precursor is physically adsorbed into the zeolite cages without further chemical reaction. As found with other carbonyl compounds, the Na^+ ions in the zeolite framework interact with the CO ligands at the oxygen end,[28] resulting in symmetry changes of the $Mn(CO)_5$ moiety. The weakly adsorbed species are preferentially removed from the zeolite with increasing temperature. The remaining complex decomposes at about 423 K by loss of CO ligands and, subsequently, cleavage of the Sn–Mn bond. Mn and Sn cluster species of unknown structure are formed at 523 K.

In contrast to the NaY host, the acidic H6Y host offers a chemically reactive surface that can interact with the Me_3Sn moiety of the bimetallic complex. Different degrees of substitution of the methyl groups by the acidic oxygen framework are observed. Both mono- and disubstituted species, $(O_z)Me_2SnMn(CO)_5$ and $(O_z)_2MeSnMn(CO)_5$, are formed in the highly proton-exchanged zeolite. The degree of substitution increases with temperature. After the Sn–Mn bond is cleaved at 423 K, tin is still anchored to the zeolite framework through oxygen coordination while unidentified Mn cluster species are formed. At 523 K, both Sn and Mn are attached to the zeolite oxygen framework.

These results show that the heterobimetallic compound $Me_3SnMn(CO)_5$ can be anchored into the cages of acidic zeolites at room temperature under retention of the Sn–Mn bond. The methyl ligands are good leaving groups in H6Y but do not react in NaY. The intrazeolite complex in NaY undergoes carbonyl substitution with PEt_3 at the manganese atom. The thermal stability of the intrazeolite, attached species permits further studies on their chemical reactivity and potential catalytic activity.

Acknowledgment. We thank Professor D. C. Koningsberger for EXAFS data analysis software. Acknowledgment is made to the donors of the Petroleum Research Fund, administered by the American Chemical Society, and to the U.S. Department of Energy (DE-FG04-90ER14158) for partial funding of this work. The operational funds for NSLS beamline X-11A are supported by DOE grant DE-AS0580ER10742.

Registry No. $Me_3SnMn(CO)_5$, 14126-94-4; PEt_3, 554-70-1; Mn, 7439-96-5; Sn, 7440-31-5.

Supplementary Material Available: Fourier-transformed EXAFS data of the reference compounds, description of the calculation of an $Mn(CO)_5$ reference, structural EXAFS analysis of the $Me_3Mn(CO)_5$ precursor, and details of the analysis of the precursor in NaY (Mn edge), and in H6Y (Sn edge) (12 pages). Ordering information is given on any current masthead page.

References and Notes

(1) Lamb, H. H.; Gates, B. C.; Knözinger, H. *Angew. Chem., Int. Ed. Engl.* **1988**, *27*, 1127.
(2) Bailey, D. C.; Langer, S. H. *Chem. Rev.* **1981**, *81*, 109.
(3) Breck, D. W. *Zeolite Molecular Sieves*; R. E. Krieger Publishing Co.: Malabar, FL, 1984.
(4) *Zeolites: Facts, Figures, Future*; Jacobs, P. A., van Santen, R. A., Eds.; *Stud. Surf. Sci. Catal. 49*; Elsevier: Amsterdam, 1989.
(5) Suib, S. L.; Kostapapas, A.; McMahon, K. C.; Baxter, J. C.; Winiecki, A. M. *Inorg. Chem.* **1985**, *24*, 858.
(6) Bein, T.; McLain, S. J.; Corbin, D. R.; Farlee, R. F.; Moller, K.; Stucky, G. D.; Woolery, G.; Sayers, D. *J. Am. Chem. Soc.* **1988**, *110*, 1801.
(7) Herron, N. *Inorg. Chem.* **1986**, *25*, 4714.
(8) Diegruber, H.; Plath, P. J.; Schulz-Ekloff, G. *J. Mol. Catal.* **1984**, *24*, 115.
(9) Davis, M. E.; Schnitzer, J.; Rossin, J. A.; Taylor, D.; Hanson, B. E. *J. Mol. Catal.* **1987**, *39*, 243.
(10) Shannon, R. D.; Vedrine, J. C.; Naccache, C.; Lefebvre, F. *J. Catal.* **1984**, *88*, 431.
(11) Rode, E. J.; Davis, M. E.; Hanson, B. E. *J. Catal.* **1985**, *96*, 574.
(12) Huang, T. N.; Schwartz, J.; Kitajima, N. *J. Mol. Catal.* **1984**, *22*, 389.
(13) Huang, T. N.; Schwartz, J. *J. Am. Chem. Soc.* **1982**, *104*, 5244.
(14) Corbin, D. R.; Seidel, W. C.; Abrams, L.; Herron, N.; Stucky, G. D.; Tolman, C. A. *Inorg. Chem.* **1985**, *24*, 1800.
(15) Taylor, D. F.; Hanson, B. E.; Davis, M. E. *Inorg. Chim. Acta* **1987**, *128*, 55.
(16) (a) Borvornwattananont, A.; Moller, K.; Bein, T. *J. Chem. Soc., Chem. Commun.* **1990**, 28. (b) Borvornwattananont, A.; Moller, K.; Bein, T. Synthesis/Characterization and Novel Applications of Molecular Sieve Materials. Bedard, R. L., Bein, T., Davis, M. E., Garces, J., Maroni, V. A., Stucky, G. D., Eds.; *Mater. Res. Soc. Symp. Proc.* **1991**, *233*, 195. (c) Borvornwattananont, A.; Moller, K.; Bein, T. *J. Phys. Chem.* **1992**, *96*, 6713.
(17) Booth, M. R.; Cardin, D. J.; Clack, H. C.; Sreenathan, B. R. *J. Organomet. Chem.* **1970**, *21*, 171.
(18) Bailar, J. C., Jr.; Emeleus, H. J.; Nyholm, R.; Trotman-Dickenson, A. F. *Comprehensive Inorganic Chemistry*; Pergamon Press: Oxford, 1973; Vol. 2, p 46.
(19) Bichler, R. E. J.; Booth, M. R.; Clack, H. C.; Hunter, B. K. *Inorg. Synth.* **1970**, *12*, 60.
(20) Hansen, M.; Anderko, K. *Constitution of Binary Alloys*, McGraw-Hill: New York, 1958; p 954.
(21) Clark, H. C.; Tsai, J. H. *Inorg. Chem.* **1966**, *5*, 1407.
(22) The Mn species are believed to be zeolite-attached Mn clusters. However, the products may also contain the Mn-rich carbide species (solid solutions of carbon in bulk manganese) such as Mn_7C_3 or $Mn_{23}C_6$ which are isomorphous to Cr_7C_3 or $Cr_{23}C_6$, respectively. The Mn–O_z or Mn–C bond in our system (1.94 Å) is slightly longer than the Mn–O bond in MnO_2 (1.89 Å; see: Ewald, Von P. P.; Hermann, C. *Zeitschrift Fur Kristallographie Kristallgeometrie, Kristallphysik, Kristallchemie*, subtitle *Strukturbericht*; Johnson Reprint Corp.: New York, 1931; Vol. 1, p 155) but shorter than the nearest Cr–C bond length (2.09 Å) in $Cr_{23}C_6$ (the unit cell parameter a = 10.638 Å; see: Gottfried, C.; Schossberger, F. *Zeitschrift Fur Kristallographie Kristallgeometrie, Kristallphysik, Kristallchemie*, subtitle *Strukturbericht*; Johnson Reprint Corp.: New York, 1937; Vol. 3, p 59) which should be similar to the Mn–C bond length in $Mn_{23}C_6$ (a = 10.61 Å; see: Hansen, M.; Anderko, K. *Constitution of Binary Alloys*; McGraw-Hill: New York, 1958; p 367). The EXAFS data of the zeolite samples could be due to overlapping contributions from several of the above species, including Mn–O_z and Mn–C (indicated by the high value of $\Delta\sigma^2$). The sources of carbon in the carbide products may be the CH_3 or CO ligands. Unidentified Sn species are also the decomposition products at 523 K.
(23) Onaka, S. *Bull. Chem. Soc. Jpn.* **1975**, *48*, 319.
(24) Bryan, R. F. *J. Chem. Soc. A* **1968**, 696.
(25) Carey, N. A. D.; Clark, H. C. *Inorg. Chem.* **1968**, *7*, 94.
(26) Gorsich, R. D. *J. Chem. Soc. A* **1962**, *84*, 2486.
(27) Corbridge, D. E. C. *Studies in Inorganic Chemistry*, subtitle *Phosphorus, An outline of its Chemistry, Biochemistry and Technology*, 3rd ed.; Elsevier: New York, 1985; Vol. 6, p 717.
(28) (a) Moller, K.; Borvornwattananont, A.; Bein, T. *J. Phys. Chem.* **1989**, *93*, 4562. (b) Borvornwattananont, A.; Moller, K.; Bein, T. *J. Phys. Chem.* **1989**, *93*, 4205.